Nonlinear interactions of multilevel atoms with a near-resonant standing wave

T. J. O'Kane,[1] R. E. Scholten,[1] P. M. Farrell,[2] and M. R. Walkiewicz[1]
[1]*School of Physics, University of Melbourne, Parkville 3052, Australia*
[2]*Optical Technology Research Laboratory, Victoria University, Footscray 8001, Australia*
(Received 9 November 1998)

Using a semiclassical density matrix formalism we have calculated the behavior of multilevel atoms interacting with a standing wave field, and show how complex nonlinear phenomena, including multiphoton effects, combine to produce saturation spectra as observed in experiments. We consider both 20-level sodium and 24-level rubidium models, contrasting these with a simple 2-level case. The influence of parameters such as atomic trajectory and the time the atom remains in the beam are shown to have a critical effect on the line shape of these resonances and the emission/absorption processes. Stable oscillations in the excited state populations for both the two-level and multilevel cases are shown to be limit cycles. These limit cycles undergo period doubling as the system evolves into chaos. Finally, using a Monte Carlo treatment, these processes average to produce saturated absorption spectra complete with power and Doppler broadening effects consistent with experiment. [S1050-2947(99)00406-0]

PACS number(s): 32.80.Pj, 42.50.Vk

I. INTRODUCTION

The interaction of a strong standing wave with an atomic system has long been a topic of considerable interest for both theorists and experimentalists. This system is at the heart of many atom optics problems ranging from the workings of a gas laser [1–3] through saturation spectroscopy [4–8], optical pumping [9–12] to laser cooling [13–15]. Early calculations considered systems of linear first-order differential equations in which the atom is stationary or moving in a constant traveling wave field with no spatial dependence. For example Balykin *et al*. [10] treat atoms interacting with a resonant incident traveling wave laser, via numerical integration of the optical Bloch equations. This formalism is semiclassical, treating the incident light field classically, and is a direct extension of the two-level model of Allen and Eberly [16]. More recently Farrell *et al*. [12] have extended this approach to include all decay terms derived from a fully quantized light field.

With the introduction of a standing wave, and atomic motion, we now have a system of coupled, first order differential equations with harmonic coefficients [17]. The atoms, moving with a thermal distribution of velocities, acquire nonlinear electric dipole moments under the action of the field. Due to the standing wave influence the respective energy level populations do not achieve the steady state solution normally induced via relaxation. Instead these parameters develop stable oscillatory motion indicative of the system evolving into a limit cycle, the signature of nonlinear, dissipative systems [18].

Analytic solutions are available for the case of a simple traveling wave interacting with a two-level system [16], and approximate perturbation solutions have been found for the strong-pump weak-probe case [19–21], in which the probe beam is considered a perturbation to the traveling wave solution. Pegg and Schulz [22] have solved the case for a two-level system with relaxation in a standing wave field via a series of basis transformations to rotating frames for particular oscillation frequencies. However, if relaxation terms are absent, there remains no analytic solution for the two-level standing wave laser-atom interaction [23].

Atoms commonly used in optical pumping experiments have many coupled levels. For example, rubidium experiments typically involve 24 states, leading to a 24×24 element density matrix, and a system of 576 coupled complex differential equations; approximation and numerical simulation are clearly necessary. The most recent work to consider optical pumping effects in high resolution laser spectroscopy [8] is based on rate equations, applied in the low intensity regime so that coherence effects could be excluded. These coherence terms become of increasing importance as the laser intensity is increased or in the case of equal intensity ''pump'' and ''probe'' beams, and determine the evolution of the nonlinear laser-atom interaction.

We have developed a detailed model using the formalism of the semiclassical density matrix equations (SDE) [11,12], solved using standard numerical techniques and Monte Carlo methods. Initially we consider a single atom moving through a Gaussian standing wave with left-hand circular (σ^+) polarization. As the atom travels through the beam its density matrix evolves according to the SDE. The density matrix then allows the calculation of parameters such as state populations, absorption and dispersion.

We show that this method allows calculation of nonlinear processes such as multiphoton resonances and their gradual saturation as laser intensity is increased. The sensitivity of these processes to the path of the atoms through the laser beam is also demonstrated. The effects of the dissipative terms in both the two-level and multilevel systems are explored. Variation of these terms can lead to limit cycles, period doubling, and chaos. Finally, a Monte Carlo treatment is adopted to average these nonlinear processes over a sample of paths and velocities representative of the atoms in a vapor cell, to produce a saturated absorption spectrum for atomic rubidium that is consistent with experiment.

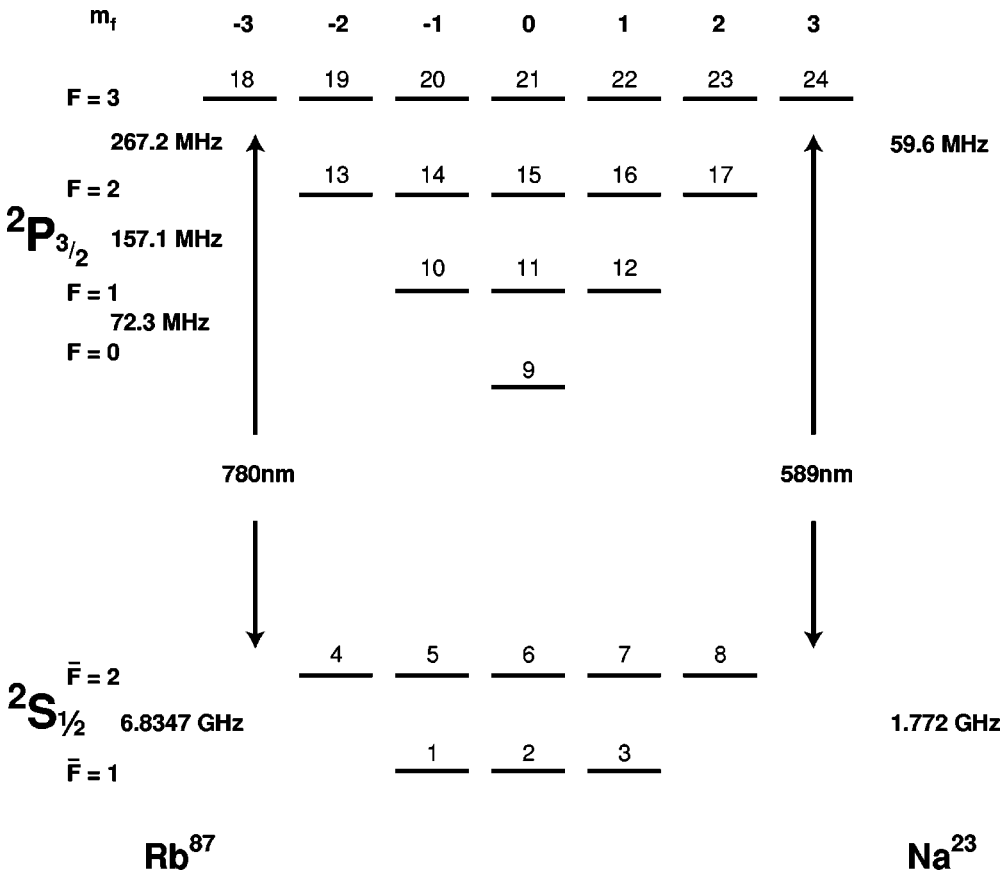

FIG. 1. Energy level diagram for the 24-level $5^2S_{1/2}$ and $5^2P_{3/2}$ states of Rb^{87} and the 20-level $3^2S_{1/2}$,$3^2P_{3/2}$ states of Na^{23}. The energy splittings are shown for Rb^{87} on the left, and for Na^{23} on the right. The excited state numbering is shown for the full 24 levels used for Rb; the $F=0$,1 excited states are omitted in the Na model.

II. THEORY

We consider a multilevel rubidium or sodium system (Fig. 1) with excited and ground-state energy levels $|e\rangle$ and $|g\rangle$ such that $E_e-E_g=\hbar\omega_0$, where ω_0 is the resonant transition frequency. Such an ensemble is readily described by an $N\times N$ density matrix [24] whose diagonals represent the populations of the respective energy levels and whose off-diagonal elements are proportional to the atomic dipole moment; N is the number of states. The system is subjected to two counterpropagating electromagnetic waves of the same angular frequency ω, propagating in opposite directions along the z axis, with σ^+ polarization relative to the z direction, the quantization axis. For a standing wave along the z axis, the electric field can be described by

$$\mathbf{E}=E\cos(kz)(\epsilon_\nu\exp(-i\omega t)+\epsilon_\nu^*\exp(i\omega t)), \tag{1}$$

where the amplitudes E of the plane waves are real.

We first define the matrix element of the interaction Hamiltonian in the dipole approximation as

$$H'_{\alpha\beta}=\sum_{\nu=\pm1,0} C^\nu_{\alpha\beta}\,\mu\mathbf{E}, \tag{2}$$

where μ is the dipole transition matrix element, $C^\nu_{\alpha\beta}$ are the Clebsch-Gordan coefficient for the $\alpha\rightarrow\beta$ transition, and α,β refer to ground and excited states, respectively. $E\epsilon_\nu$ is the electric field strength at polarization ϵ_ν, where $\nu=\pm1$ for $\sigma^\pm$ circular polarization, and 0 for linear polarization, respectively. The quantity μE is given by

$$\mu E=\frac{\hbar}{\tau}\sqrt{\frac{I_0}{2I_{\rm sat}}}, \tag{3}$$

where I_0 is the traveling wave laser intensity and $I_{\rm sat}$ the saturation intensity. For a Gaussian beam standing wave, we similarly define $\mu E'(r,z)$, replacing I_0 with the laser intensity given by

$$I(r,z)=4I_0\cos^2(kz)\exp\left(\frac{-2r^2}{l_{\rm rad}^2}\right). \tag{4}$$

I_0 is the peak laser intensity of a single traveling wave beam, $k=2\pi/\lambda_{\rm laser}$ where $\lambda_{\rm laser}$ is the laser wavelength, and $l_{\rm rad}$ is the beam radius, set at 1 mm. Radius r is the distance perpendicular to the standing wave beam. The natural lifetime of the transition, τ, is 16.237 ns for sodium [25] and 25.8 ns for rubidium [26].

The time evolution of the density matrix is given by

$$\frac{d\rho_{\alpha\beta}}{dt}=-i\omega_{\alpha\beta}\rho_{\alpha\beta}-\frac{i}{\hbar}\sum_\gamma\,(H'_{\alpha\gamma}\rho_{\gamma\beta}-\rho_{\alpha\gamma}H'_{\gamma\beta}) \tag{5}$$

to which we add phenomenological decay terms in the semiclassical style [12,16]. For rubidium, there are $24^2=576$ coupled differential equations, with coefficients that have a

cosinusoidal dependence on time. We invoke the rotating wave approximation, defining slowly varying off-diagonal components $\tilde{\rho}_{\alpha\beta}$ by $\rho_{\alpha\beta}=\tilde{\rho}_{\alpha\beta}\exp(i\omega t)$ and eliminate terms that oscillate at twice the optical frequency [16]. We also exclude all off-diagonal terms that do not couple an excited state to a ground state, that is where $\Delta F\neq 0,\pm 1$ and (for σ^+ polarization) $\bar{m}+1\neq m$. Note that the QED model of Farrell *et al.* [12] includes additional terms coupling between the vertical coherences of the excited state levels. These are omitted since they are of crucial importance only in the regime of very high laser intensity which for the case of rubidium would require a laser intensity at least an order of magnitude greater than those we have considered. We also ignore coupling between magnetic sublevels of the same F level as well as off diagonals that couple the $\bar{F}=1$ ground state to the excited states. These terms become significant only at laser intensities that allow large power broadening of the $\bar{F}=1,F=0$ (rubidium model), $\bar{F}=1,F=2$ (sodium model) transitions such that the amplitude is significant at ω_0, or for two frequency pumping [27]. Finally Hermiticity (i.e., $\rho_{\alpha\beta}=\rho^*_{\beta\alpha}$) halves the number of remaining equations, leaving the following final set of equations for the rubidium system:

$\bar{F}=1$ ground-state diagonals:

$$\frac{d\rho_{\alpha\alpha}}{dt}=\frac{1}{\tau}\sum_{\nu=0,\pm 1}\sum_{\beta=9}^{17}(C^{\nu}_{\alpha\beta})^2\rho_{\beta\beta}. \tag{6}$$

$\bar{F}=2$ ground-state diagonals:

$$\frac{d\rho_{\alpha\alpha}}{dt}=-\frac{\mu E'(r,z)}{\hbar}\sum_{\beta=9}^{24}\epsilon_{+1}C^{+1}_{\alpha\beta}\mathrm{Im}(\tilde{\rho}_{\alpha\beta})+\frac{1}{\tau}\sum_{\nu=0,\pm 1}\sum_{\beta=9}^{24}(C^{\nu}_{\alpha\beta})^2\rho_{\beta\beta}. \tag{7}$$

Excited-state diagonals:

$$\frac{d\rho_{\beta\beta}}{dt}=\frac{\mu E'(r,z)}{\hbar}\sum_{\alpha=4}^{8}\epsilon_{+1}C^{+1}_{\beta\alpha}\mathrm{Im}(\tilde{\rho}_{\beta\alpha})-\frac{1}{\tau}\rho_{\beta\beta}. \tag{8}$$

Off diagonals:

$$\frac{d\tilde{\rho}_{\alpha\beta}}{dt}=\frac{i\mu E'(r,z)}{2\hbar}\epsilon_{+1}C^{+1}_{\alpha\beta}(\rho_{\alpha\alpha}-\rho_{\beta\beta})+i(\omega_{\alpha\beta}-\omega)\tilde{\rho}_{\alpha\beta}-\frac{1}{2\tau}\tilde{\rho}_{\alpha\beta}. \tag{9}$$

The numerical solution of these equations is carried out by use of Runge-Kutta techniques with the initial populations evenly distributed among the ground-state diagonals and all other elements of the density matrix zero. Note that the radius r and longitudinal position z are not independent: they are determined from the velocity and angle of the atomic trajectory. The time steps through the numerical routine must be considerably smaller than the inverse of any of the radiative processes, i.e., $dt\ll\Gamma^{-1},\Omega^{-1},\Delta^{-1}$ where Γ is the atomic decay rate, $\Omega=\mu E'/\hbar$ the Rabi frequency, and Δ the total detuning including Doppler shift; thus we are limited to step sizes of approximately 0.1 ns. This is the main restriction in terms of computation time and, coupled with instability induced by the spatially dependent driving terms due to the standing wave, makes the moving atom model very intensive computationally.

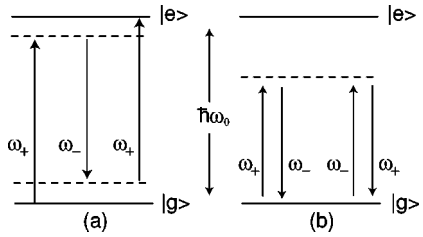

FIG. 2. The first-order multiphoton transitions in the two-level model. (a) corresponds to the laser being far from resonance. Through the absorption of two photons from one of the component waves of the standing wave field ω_+ simultaneously with stimulated reemission of one photon of the counterpropagating field ω_- the atoms may be excited from the ground to the excited state, i.e., a Raman transition. It is because this process is related to stimulated emission that negative absorption (emission) may take place. (b) represents the two possible Rayleigh processes which correspond to the even resonances in the diagonals of the density matrix.

III. MULTIPHOTON RESONANCES AND THE SATURATION PROCESS

In the rest frame of an atomic ensemble moving with a given velocity v_z, the applied standing wave field appears as a pair of counterpropagating traveling wave components of frequencies $\omega_\pm=\omega\mp kv_z$. Provided their frequency separation is of order less than or equal to the atomic relaxation rate, i.e.,

$$|\omega_+-\omega_-|=2k|v_z|\leqslant\Gamma_e+\Gamma_g, \tag{10}$$

where $\Gamma_e=\Gamma_g=1/\tau$ are the excited and ground-state relaxation rates, the field components couple parametrically, generating components of induced polarization at sideband frequencies $\omega\pm kv_z/n$, $n=1,3,5,\ldots$. These in turn react back, influencing the polarization at the fundamental frequency $\omega\pm kv_z$. The sideband frequencies correspond physically to multiphoton resonances [Fig. 2(a)] and have been calculated for two-level systems via perturbation techniques [21] and continued fractions [4], and for RF resonances, using Floquet theory [28,29]. There are also even resonances [Fig. 2(b)] in the populations i.e., $2,4,\ldots,n$-photon transitions, resulting from absorption of a photon from one of the component traveling waves simultaneous with stimulated emission into the counterpropagating traveling wave. Energy conservation dictates that these ground to ground-state transitions occur for zero velocity atoms: $(\omega\pm kv_z)-(\omega\mp kv_z)=0$. After briefly discussing the two-level case we provide calculations of these nonlinear processes for multilevel systems.

A. Two-level systems

For simplicity we first consider the case of a two-level atom moving through a Gaussian standing wave beam. An atom with given velocity v is fired at angle θ, with respect to

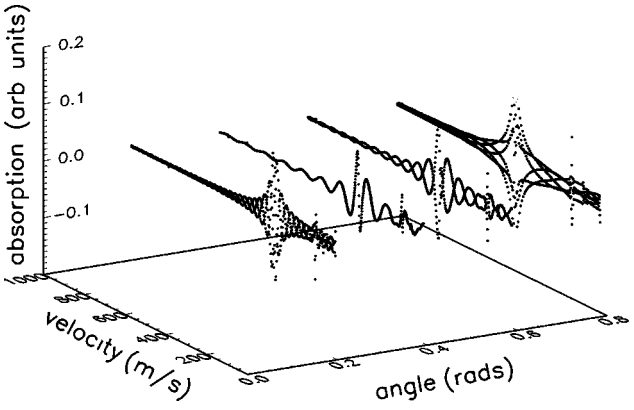

FIG. 3. Absorption versus atomic velocity for two-level sodium atoms. Two-level atoms, modeled on the $\overline{F}=2$ ground$\rightarrow F=3$ excited state transition in atomic sodium, are fired at velocity increments of 1 m/s, respectively. The absorption is given by $\mathrm{Im}\{\mathrm{Tr}(C^{\nu}_{\alpha\beta}\,\rho_{\beta\alpha})\}$ and is plotted against the atomic velocity. The internal structure evident in the absorption ''envelope'' is due to the sampling rate, which corresponds to the taking of a measurement at a particular point in the standing wave, while the symmetry about the absorption axis is due to induced dipolelike oscillation in the coherences due to motion through the nodes. The laser is set at twice saturation intensity ($I_0=12$ mW/cm^2) and detuned 500 MHz from resonance. The angles considered are $\pi/16,\pi/8,3\pi/16,\pi/4$ and the clearly defined resonances correspond to 1, 3, 5, and 7 photon processes. The primary resonance is a linear process and provides a reference with which to analyze the absorptive/emissive nature of higher order nonlinear processes.

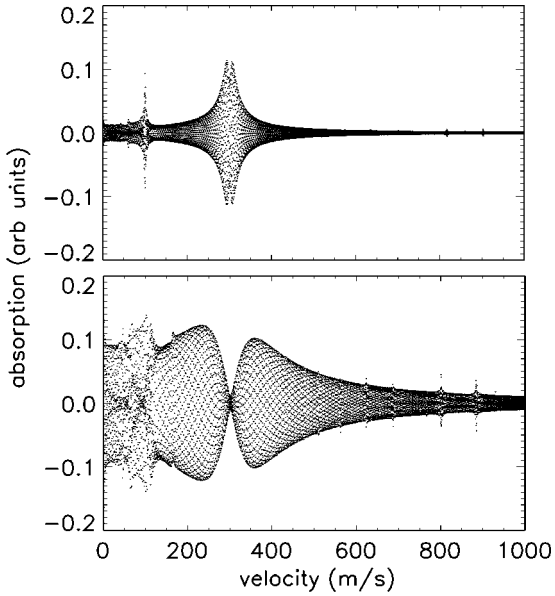

FIG. 4. Absorption versus atomic velocity. If we now decrease the velocity increment to 0.1 m/s for the $\pi/16$ path (upper) we obtain a clearly resolved calculation of the absorption envelope with the primary resonance clearly saturated ($I_0=12$ mW/cm^2, 500 MHz detuned). For 2-level atoms fired directly down the standing wave field (lower) with peak intensity set at $I_0=1$ W/cm^2 we again see that the primary and 3-photon resonances have become saturated. Power broadening and strong resonance effects at velocities above the primary resonance induce nonlinear atom-field couplings, as indicated by the minor peaks. The absence of fine structure in the region of the 3, 5, and 7 photon resonances is clearly intensity dependent and indicates a high level of instability in the coherences for slow moving atoms, induced via motion between the nodes.

the laser beams, through a standing wave field of σ^+ polarization and the absorption is then calculated after the atom either exits the beam or after sufficient time has elapsed such that the atom has reached stable behavior. We calculate the absorption as for a traveling wave, using $\mathrm{Im}\{\mathrm{Tr}(C^{\nu}_{\alpha\beta}\rho_{\alpha\beta})\}$. For a standing wave, the absorption is more appropriately calculated from the state populations, as discussed in Sec. V, but these hide many interesting nonlinear effects we wish to consider here.

The calculation is repeated for a range of initial velocities, thus obtaining all possible absorptions for a given path through the beam. In Fig. 3 we present the results of such a simulation for a two-level atom modeled on the $\overline{F}=2\rightarrow F=3$ transition for sodium with the laser intensity set at twice saturation intensity ($I_0=12$ mW/cm^2), detuned from resonance by 500 MHz ($\sim$300 m/s) at incremented angles to the beam. We clearly see the saturated primary resonance as well as the three- and to a lesser extent the 5-photon processes. The oscillations between positive and negative absorptions correspond to the position of the atom in the standing wave field at the time the measurement is taken and result from the atoms emitting and absorbing photons in different regions of the field. The symmetry of the data results from oscillations in the coherences as the atoms travel through the modulated standing wave intensity. These oscillations are dependent on the strength of the relaxation terms as well as the trajectory through the beam, the beam intensity and the amount of time the atom spends in the beam. If we decrease the rate at which we increment each atom's velocity, we can measure the full envelope of the absorption (Fig. 4).

The primary resonance is a linear process [21] while the higher order resonances are a result of the nonlinear atom-field coupling. By increasing the laser intensity to $I_0=1$ W/cm^2 we see clear evidence of saturation at the primary and three-photon resonances as well as power broadening (Fig. 4). We also see an increase in the strength of the higher order resonances as well as resonances occurring for atoms with large velocities due to nonlinear couplings of the field and atom. The lack of structure for slow moving atoms at velocities corresponding to the higher order processes is a clear indication of intensity induced instability in the coherences.

B. 20-level sodium

Next we consider a 20-level sodium model ($F=0,1$ hyperfine levels omitted) in which atoms are fired through the standing wave field at an angle of $\pi/8$ to the direction of propagation (Fig. 5). The calculation for an atom is terminated when the trajectory carries it out of the laser path, or after 200 lifetimes. At saturation intensity ($I_0=6$ mW/cm^2) the 1-, 3-, and 5-photon processes are observed with the 3- and 5-photon processes clearly emissive. As the laser intensity is increased the primary and tertiary resonances becomes saturated. The strength of the 5-photon resonance is also enhanced and saturated. A comparison of the $\pi/8$ path for the 2-level (Fig. 3) and multilevel (Fig. 5) cases reveal the 3-photon process being of opposite sign.

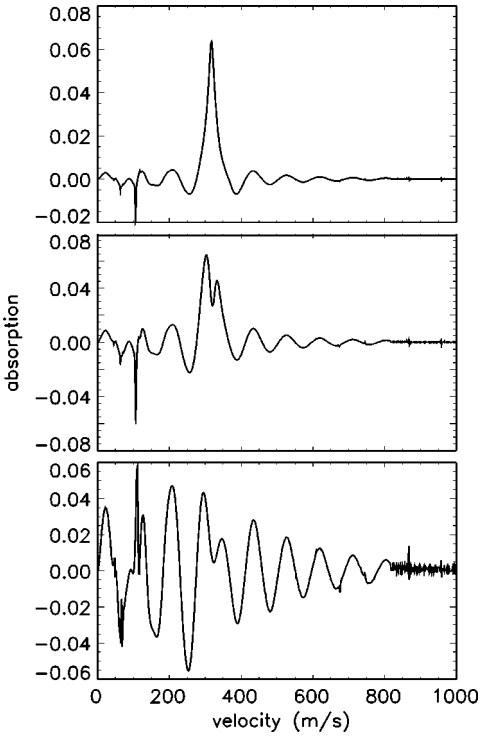

FIG. 5. Absorption versus atomic velocity for 20-level sodium atoms. The absorption for a 20-level sodium model with atoms selected at the same position (relative to any given pair of nodes) and dipole moment in the field. The angle to the beam θ is set at $\pi/8$ and the laser detuned by 500 MHz. Laser intensities considered are $I_0=6$ mW/cm^2 (upper), 54 mW/cm^2 (middle), and 1 W/cm^2 (lower). As for the two-level model we see the odd multiphoton resonances with the 3-, 5-photon processes clearly emissive as opposed to the 2-level calculation (Fig. 3, $\theta=\pi/8$) demonstrating the influence of the related coherences. At 1 W/cm^2 the 1-, 3-, and 5-photon resonances are saturated and the 5- and 7-photon processes enhanced. The 3-photon process is now clearly absorptive while the 7-photon process is dispersive indicating intensity dependence in the higher order processes. The hyperfine resonance is present at $I_0=6$ mW/cm^2 but is weak due to the small splitting (59 MHz) for the $F=2\rightarrow F=3$ excited states. The 20-level sodium model omits the $F=0,F=1$ hyperfine states.

This result is due to the absence of the extra coherence terms in the two-level model and is clear indication for the necessity of multilevel calculations when dealing with ''real'' atoms. At 1 W/cm^2 the 3-photon process becomes absorptive while the 7-photon process becomes dispersive.

IV. STABILITY OF THE DENSITY MATRIX EVOLUTION

The coherences determine the behavior of processes such as absorption, dispersion, and polarization and it is important to have some understanding of the nature of their oscillatory behavior. Phase-space simulations of the 2-level Bloch vector equation reveal that the system initially obeys the steady oscillatory behavior of a limit cycle. The Bloch vector is defined as (u,v,w) where [16]

$$u=(\tilde{\rho}_{\alpha\beta}+\tilde{\rho}_{\beta\alpha}), \tag{11}$$

$$v=i(\tilde{\rho}_{\beta\alpha}-\tilde{\rho}_{\alpha\beta}), \tag{12}$$

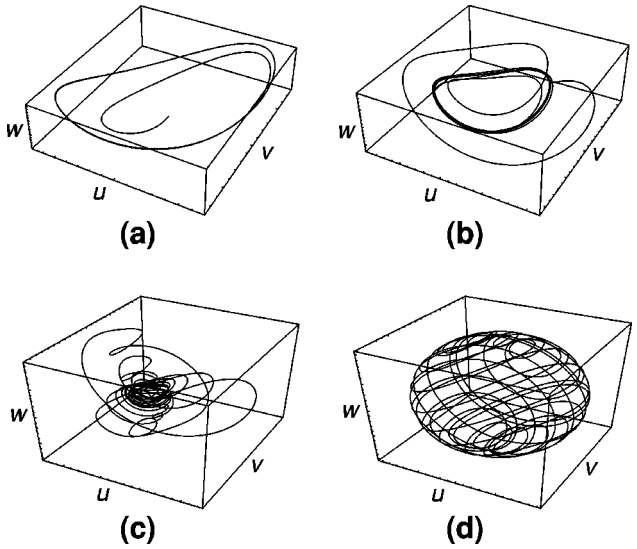

FIG. 6. Parameter space plots of the two-level Bloch vector equation for an idealized dimensionless atom showing the effects of a reduction in the relaxation terms. As the strength of the relaxation terms are reduced the stable limit cycle induced by the counterpropagating fields unravels evolving to chaotic motion on the Bloch sphere for zero relaxation. This is in contrast to the traveling wave case (at zero detuning) in which the system oscillates at the Rabi frequency corresponding to evolution in a closed circle (geodesic) on the Bloch sphere. The relaxation is reduced by factors of 1, 0.1, 0.01, and 0 for (a)–(d), respectively.

$$w=(\rho_{\beta\beta}-\rho_{\alpha\alpha}). \tag{13}$$

As we reduce the rate of relaxation (Γ), equivalent to increasing the laser intensity but much faster computationally, the limit cycle ''unravels'' until the system reaches fully chaotic behavior on the Bloch sphere (Fig. 6). A suitable transformation of variables such as first reported by Haken [30] shows the system to be identical to the Lorenz equations with cosinusoidal driving terms added [31]. This chaotic behavior in a self-oscillating system [32] was first reported by Silverberg and Bar-Joseph [33] for the case of counterpropagating waves interacting in a third-order nonlinear medium and then extended to the two-level atom steady state case [34]. There is also strong evidence that this system follows a period doubling route to chaos, but we have not attempted to classify it.

In Fig. 7 we show the $F=3,m_f=3$ excited state population for the 20-level sodium model at saturation intensity. We clearly see the stable oscillations of a period 1 limit cycle, due to atomic motion through the nodes of the field. The system evolves from Rabi oscillations through the optical pumping phase and steady convergence to stable behavior. In phase space, we see stable orbits (Fig. 8), indicating the system has converged to a limit cycle in *n*-dimensional parameter space, where *n* is the number of differential equations needed to parametrize the system. As we increase the intensity to $I_0=54$ mW/cm^2 it is evident that the limit cycle has undergone period doubling with the associated coherence now displaying a complicated but stable orbit (Fig. 9). At $I_0=1$ W/cm^2 the Rabi oscillations are very intense as evident in the large oscillations in the early stages of the phase portrait (Fig. 7). As intensity is increased the number of pe-

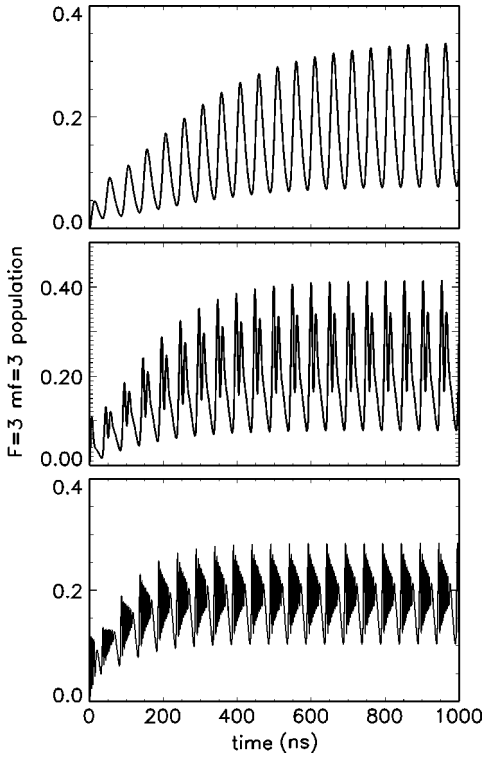

FIG. 7. Sodium $F=3,m_f=3$ excited state population versus time. With $I_0=6$ mW/cm^2 (upper) for an on-resonance atom traveling at 5.9 m/s (10 MHz detuned) down the field the large stable oscillations are induced by motion through the field nodes. At $I_0=54$ mW/cm^2 (middle) a secondary oscillation is induced due to atomic motion between the nodes. Finally at $I_0=1$ W/cm^2 (lower) large intensity dependent population oscillations are apparent.

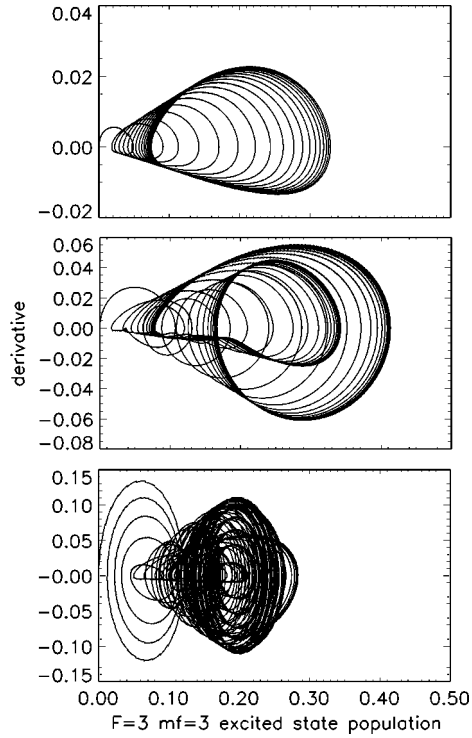

FIG. 8. $F=3,m_f=3$ excited state population versus its derivative: $\rho(20,20)$ vs $(d/dt)\rho(20,20)$ (parameters as for Fig. 7). After initial Rabi oscillations and optical pumping a stable period-1 limit cycle is reached at saturation intensity (upper). At $I_0=54$ mW/cm^2 (middle) the effects of the higher intensity are manifest in the sodium population limit cycle now having period-2 after undergoing period doubling. The $\overline{F}=2,m_f=2$ population displays an inverse relation to the $F=3,m_f=3$ population, as expected due to the circular polarization. For $I_0=1$ W/cm^2 (lower) the $\rho(20,20)$ population evolution for sodium clearly demonstrates the effects of amplitude modulation due to the standing wave. We note that the system settles into stable period-9 behavior.

riods in the limit cycle also increases, as observed in the ''unraveling'' of the two-level Bloch vector calculations, and it is apparent that the system will ultimately become chaotic for sufficiently large laser intensity. This is in part due to the dipolelike behavior of the off diagonals in the density matrix where the period of the coherence limit cycles are significantly higher and therefore more sensitive to intensity, indicative of the time dependence of the off-diagonal matrix elements. The period doubling arises from intensity dependent oscillations caused by motion between the nodes.

Slowly moving atoms ''see'' the modulated laser field between the nodes, whereas fast moving atoms really only experience pertubations due to motion through the nodes. We note this effect for example in considering the effect of detuning for effectively on-resonance atoms; that is, those atoms Doppler-shifted into resonance with the detuned laser. If we contrast the oscillating standing wave case against the linear traveling wave case, for atoms Doppler-shifted into resonance at various detunings, we see these oscillations become more intense as the laser detuning is decreased. For large detunings the oscillations decrease and the behavior of the populations for the atoms in the standing wave approaches that of the traveling wave model. For resonant atoms at small detunings (i.e., slow atoms) however we find the oscillations of the limit cycle are very large, causing large variations in the final excited state populations.

If again we consider the two-level Bloch vector equation, as we reduce the relaxation time we can observe induced chaotic behavior in the coherences, while the populations remain remarkably stable, as evident in the multilevel system. This chaotic behavior evidently dissipates over time due to the effect of the remaining relaxation terms but the larger the instability in the system the longer the atom must be allowed to remain in the beam before some form of regular behavior is attained. This behavior is analogous to the loss of the fine structure in the 2-level case (Fig. 4) at high laser intensity corresponding to chaotic evolution in the coherences for the higher order photon resonances.

V. FLUORESCENCE AS ABSORPTION

The traveling-wave absorption, normally calculated from the density matrix as $\mathrm{Im}\{\mathrm{Tr}(C^{\nu}_{\alpha\beta}\rho_{\beta\alpha})\}$, is determined by the off-diagonal coherences, $\rho_{\alpha\beta}$ $(\alpha\neq\beta)$. These terms average to zero in the standing wave because the atom sees a modulated intensity as it passes through the nodes and antinodes of the field [22]. We are concerned with averages over time periods corresponding to detector bandwidths typically used in saturated absorption measurements, i.e., of order milliseconds. In this case, the total fluorescence emitted from the atoms is a more appropriate measure of the effective absorption [35,36]. We use the fluorescence normalized to the total

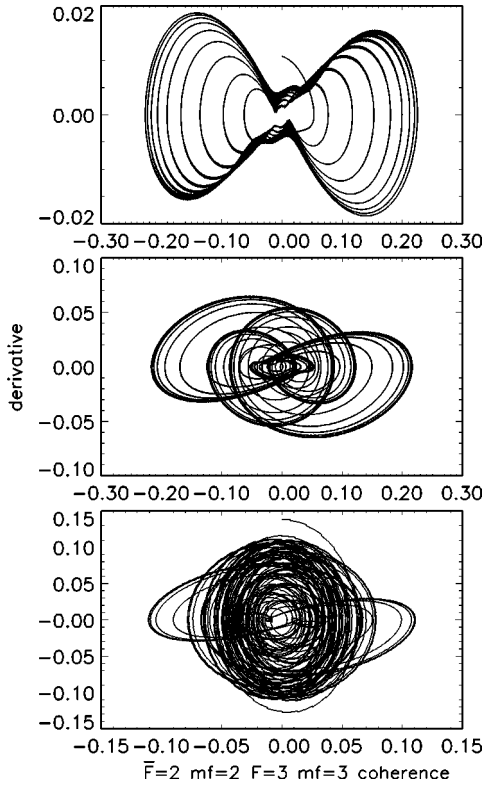

FIG. 9. $\rho(8,20)$ coherence versus $(d/dt)\rho(8,20)$ (parameters as for Fig. 7). While the coherence oscillations are still stable and symmetric at low intensity they are of a significantly higher order than the populations; i.e., initially at saturation intensity (upper) the coherence limit cycle is of the same period as those of the populations, however at $I_0=54$ mW/cm^2 (middle) the coherence phase portrait displays period 4, double that of the excited state population, indicating a higher degree of sensitivity to intensity. Significantly at $I_0=1$ W/cm^2 (lower) the coherences are highly unstable due to motion between the nodes with the system unable to reach stable behavior.

decay rate, calculated from $F=\Sigma_\beta F_\beta$ where F_β is the fluorescence due to decay from a given excited state β,

$$F_\beta=\sum_\alpha (C^\nu_{\alpha\beta})^2\rho_{\beta\beta}. \tag{14}$$

For a σ^+ circularly polarized field on resonance, the atoms are optically pumped into the $\overline{F}=2,m_f=2$ ground and $F=3,m_f=3$ excited states. The fluorescence is due to spontaneous emission only, so that for a σ^+ circularly polarized field we can regard the populations of the ''pumped'' states as a good measure of the total fluorescence and hence absorption. Note that the Monte Carlo averaging of the atom trajectories means that the excited state population is measured at random times during the density matrix evolution, and so the effects of the transients are incorporated. The validity of our choice is confirmed in Fig. 10 where we see the characteristic line shape of the multiphoton resonances and hyperfine structure in the $\overline{F}=2,m_f=0,1,2$ ground-state populations for the 24-level rubidium system.

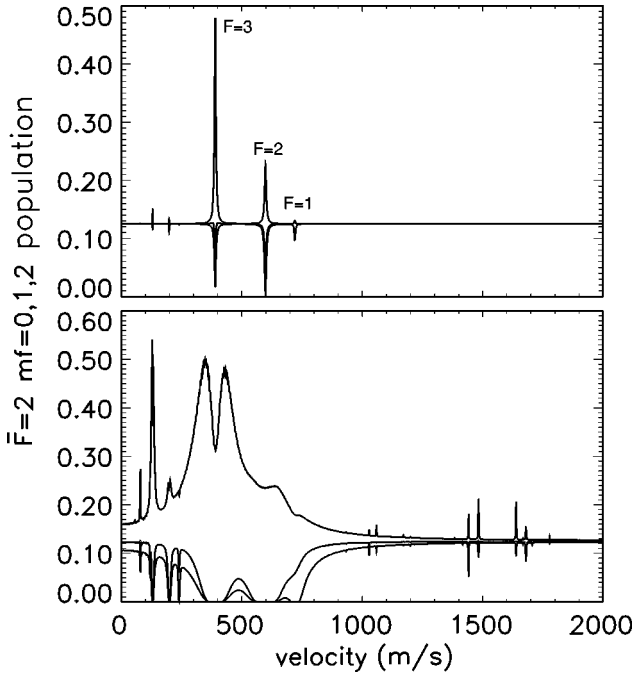

FIG. 10. $\overline{F}=2,m_f=0,1,2$ ground-state populations versus atomic velocity in Rb^{87}. Calculations for the $\overline{F}=2,m_f=0,1,2$ populations in atomic rubidium with the laser 500 MHz above resonance and intensities of $I_0=1.65$ mW/cm^2 (saturation) (upper) and 1 W/cm^2 (lower), respectively. We now see not only the resonances due to multiphoton processes but the excited state hyperfine resonances are evident due to their large energy separations in rubidium.

VI. ABSORPTION SPECTRA

In a typical experiment, such as the measurement of a saturated absorption spectrum, all of the nonlinear processes described above are lost through the inherent averaging over all the atomic velocities involved. In order to test our calculation, we average over this velocity range to produce a theoretical calculation of a power broadened and Doppler broadened saturated absorption spectrum for the rubidium model.

The absence of nonlinear processes in the linear model (i.e., traveling wave case) allows us to reduce computation time dramatically by selecting only those atoms that are on or close to resonance with the incident beam. In the standing wave case we must consider all atoms in the simulation to allow not only for power-broadening and saturated multiphoton resonances but also for induced field-atom couplings at velocities far from resonance.

We generate a Maxwell-Boltzmann distribution of velocities and random trajectories through the Gaussian beam. The laser is then set at incremented detunings and the density matrix calculated and averaged for many atoms at each respective detuning. The $F=3,m_f=3$ excited state population is used as a measure of the absorption. Figure 11 shows the saturated absorption spectrum obtained for rubidium with 10^4 atoms per detuning and a maximum time in the beam of 200 lifetimes, at a peak beam intensity of $I_0=500$ mW/cm^2. The hyperfine and crossover resonances are merged and shifted due to power broadening. This theoretical result is then compared to our own experimental re-

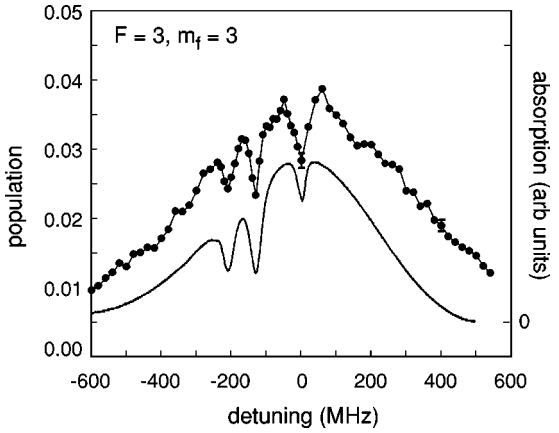

FIG. 11. Comparison of theory and experiment, showing the $F=3, m_f=3$ excited state population versus detuning for Rb^{87}. Theoretical calculation of saturated absorption spectra for rubidium with laser intensity set at $I_0=500$ mW/cm^2 thereby generating large power and Doppler broadening effects. 10 000 atoms with a Maxwellian distribution of velocities are fired at random angles θ through the beam and their density matrices averaged. The maximum time an atom can remain in the beam is 200 lifetimes and the laser is tuned to the $\overline{F}=2 \rightarrow F=3$ transition. The strength and position of the hyperfine resonances are consistent with experiment even for such small sample numbers. The experiment and theory data are displaced vertically for clarity. Typical statistical uncertainties of one standard deviation are shown at detunings of zero and +400 MHz.

sults for approximately the same laser intensity. The experiment (Fig. 12) uses a standard saturated absorption configuration.

In the case of a slow moving atom traveling at a small angle to the beam, we must arbitrarily decide when to terminate the calculation of the density matrix. Large oscillations in the populations at small laser detuning require many times more atoms to obtain resolution of the hyperfine and crossover resonances. Thus the power broadened case was chosen

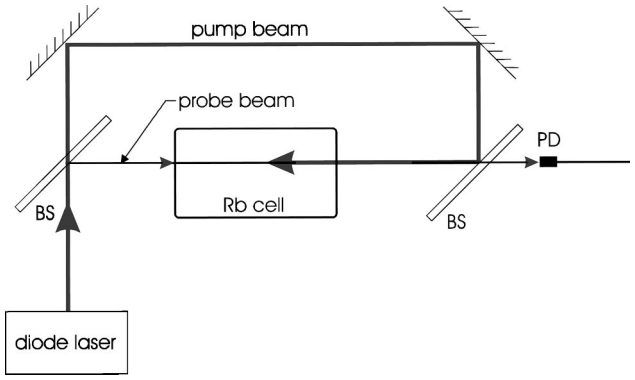

FIG. 12. Experimental configuration. BS=beam splitter, PD =photodiode detector. Cell length 40 mm; temperature 22 °C. Tuneable diode laser with linewidth 300 kHz. The beam was elliptical, 0.6 mm×0.7 mm($1/e^2$), and circularly polarized, with $I_0 \approx 630$ mW/cm^2.

to minimize the number of atoms required to produce a well resolved saturation spectrum. For saturation intensity we have been able to resolve the hyperfine and crossover resonances in the sodium model, with the crossover showing clearly as expected.

VII. CONCLUSION

The nature of the atom-laser coupling for a multilevel atom moving through a standing wave field is highly complex. We demonstrate that the statistical averages usually measured with such systems hide a rich variety of unexpected phenomena. The sensitivity of processes such as multiphoton resonances to parameters like path and time of flight has been seen to determine the line shape of the resonance.

ACKNOWLEDGMENTS

We gratefully acknowledge the support of the Australian Research Council and the Australian Postgraduate Research Awards Scheme (T.J.O., M.R.W.).

[1] W.E. Lamb, Jr., Phys. Rev. **134**, A1429 (1964).
[2] H.K. Holt, Phys. Rev. A **2**, 233 (1970).
[3] S. Stenholm and W.E. Lamb, Jr., Phys. Rev. **181**, 618 (1969).
[4] B.J. Feldman and M.S. Feld, Phys. Rev. A **1**, 1375 (1970).
[5] J.H. Shirley, Phys. Rev. A **8**, 347 (1973).
[6] B.R. Mollow, Phys. Rev. A **5**, 2217 (1972).
[7] S. Stenholm, J. Phys. B **7**, 1235 (1974).
[8] S. Nakayama, Phys. Scr. **T70**, 64 (1997).
[9] M. Ducloy, Phys. Rev. A **8**, 1844 (1973).
[10] V.I. Balykin, Opt. Commun. **33**, 31 (1981).
[11] J.J. McClelland and M.H. Kelley, Phys. Rev. A **31**, 3704 (1985).
[12] P.M. Farrell, W.R. MacGillivray, and M.C. Standage, Phys. Rev. A **37**, 4240 (1988).
[13] J. Dalibard and C. Cohen-Tannoudji, J. Opt. Soc. Am. B **6**, 2023 (1989).
[14] K. Mölmer, Phys. Scr. **45**, 246 (1992).
[15] V.G. Minogin and V.S. Letokhov, *Laser Light Pressure on Atoms* (Gordon and Breach, New York, 1987).
[16] L. Allen and J.H. Eberly, *Optical Resonance and Two-level Atoms* (Wiley, New York, 1975).
[17] C. Cohen-Tannoudji, in *Fundamental Systems in Quantum Optics*, Les Houches, Session LIII, edited by J. Dalibard, J.-M. Raimond, and J. Zinn-Justin (North-Holland, Amsterdam, 1992), pp. 1–161.
[18] A.J. Lichtenberg and M.A. Lieberman, *Regular and Stochastic Motion* (Springer-Verlag, New York, 1983).
[19] E.V. Bakalanov and V.P. Chebotaev, Zh. Éksp. Teor. Fiz. **60** 552 (1971) [Sov. Phys. JETP **33**, 300 (1971)].
[20] E.V. Bakalanov and V.P. Chebotaev, Zh. Éksp. Teor. Fiz. **62** 541 (1972) [Sov. Phys. JETP **35**, 287 (1972)].
[21] S. Haroche and F. Hartmann, Phys. Rev. A **6**, 1280 (1972).
[22] D.T. Pegg and W.E. Schulz, J. Phys. B **17**, 2233 (1984).
[23] S.M. Barnett and P.M. Radmore, *Methods in Theoretical Quantum Optics* (Clarendon Press, Oxford, 1997).

[24] K. Blum, *Density Matrix Theory and Applications, 2e* (Plenum Press, New York, 1996).
[25] C.W. Oates, K.R. Vogel, and J.L. Hall, Phys. Rev. Lett. **76**, 2866 (1996).
[26] G. Belin, Phys. Scr. **4**, 269 (1971).
[27] G. Baum, C.D. Caldwell, and W. Schröder, Appl. Phys. **21**, 121 (1980).
[28] J.H. Shirley, Phys. Rev. **138**, B979 (1965).
[29] W.M. Rutyen, Phys. Rev. A **56**, 737 (1997).
[30] H. Haken, Phys. Lett. **53A**, 77 (1975).
[31] P.W. Milonni, M-L Shih, and J.R. Ackerhalt, *Chaos in Laser-Matter Interactions* (World Scientific, Singapore, 1987).
[32] U. Parlitz, Int. J. Bifurcation Chaos Appl. Sci. Eng. **3**, 703 (1993).
[33] Y. Silverberg and I. Bar-Joseph, Phys. Rev. Lett. **48**, 1541 (1982).
[34] I. Bar-Joseph and Y. Silverberg, Phys. Rev. A **36**, 1731 (1987).
[35] C. Cohen-Tannoudji and S. Reynard, *Proceedings of the International Conference on Multiphoton Processes*, University of Rochester (Wiley, New York, 1978), p. 103.
[36] C. Cohen-Tannoudji and S. Reynard, J. Phys. B **10**, 345 (1977).